Alternative Splicing in the Voltage-Sensing Region of N-Type $Ca_V2.2$ Channels Modulates Channel Kinetics

Yingxin Lin, Stefan I. McDonough and Diane Lipscombe

J Neurophysiol 92:2820-2830, 2004. First published 16 June 2004; doi:10.1152/jn.00048.2004

Journal of Neurophysiology publishes original articles on the function of the nervous system. It is published 12 times a year (monthly) by the American Physiological Society, 9650 Rockville Pike, Bethesda MD 20814-3991. ISSN: 0022-3077, ESSN: 1522-1598. Visit our website at http://www.the-aps.org/.

J Neurophysiol 92: 2820–2830, 2004.
First published June 16, 2004; 10.1152/jn.00048.2004.

Alternative Splicing in the Voltage-Sensing Region of N-Type $Ca_V2.2$ Channels Modulates Channel Kinetics

Yingxin Lin,[1,*] Stefan I. McDonough,[2,*] and Diane Lipscombe[1,*]
[1]*Department of Neuroscience, Brown University, Providence, Rhode Island 02912; and* [2]*Marine Biological Laboratory, Woods Hole, Massachusetts 02543*

Submitted 14 January 2004; accepted in final form 14 June 2004

Lin, Yingxin, Stefan I. McDonough, and Diane Lipscombe. Alternative splicing in the voltage-sensing region of N-type $Ca_V2.2$ channels modulates channel kinetics. *J Neurophysiol* 92: 2820–2830, 2004. First published June 16, 2004; 10.1152/jn.00048.2004. The $Ca_V2.2$ gene encodes the functional core of the N-type calcium channel. This gene has the potential to generate thousands of $Ca_V2.2$ splice isoforms with different properties. However, the functional significance of most sites of alternative splicing is not established. The IVS3-IVS4 region contains an alternative splice site that is conserved evolutionarily among $Ca_V\alpha_1$ genes from *Drosophila* to human. In $Ca_V2.2$, inclusion of exon 31a in the IVS3-IVS4 region is restricted to the peripheral nervous system, and its inclusion slows the speed of channel activation. To investigate the effects of exon 31a in more detail, we generated four tsA201 cell lines stably expressing $Ca_V2.2$ splice isoforms. Coexpression of auxiliary $Ca_V\beta$ and $Ca_V\alpha_2\delta$ subunits was required to reconstitute currents with the kinetics of N-type channels from neurons. Channels including exon 31a activated and deactivated more slowly at all voltages. Current densities were high enough in the stable cell lines co-expressing $Ca_V\alpha_2\delta$ to resolve gating currents. The steady-state voltage dependence of charge movement was not consistently different between splice isoforms, but ON gating currents from the exon 31a-containing $Ca_V2.2$ isoform decayed with a slower time course, corresponding to slower movement of the charge sensor. Exon 31a-containing $Ca_V2.2$ is restricted to peripheral ganglia; and the slower gating kinetics of $Ca_V2.2$ splice isoforms containing exon 31a correlated reasonably well with the properties of native N-type currents in sympathetic neurons. Our results suggest that alternative splicing in the S3-S4 linker influences the kinetics but not the voltage dependence of N-type channel gating.

INTRODUCTION

Calcium is a ubiquitous second messenger that regulates a wide range of cellular functions. In all excitable cells, voltage-gated calcium channels couple membrane depolarization to calcium entry. Functional and structural diversity among voltage-gated calcium channels is an important mechanism employed by cells to optimize calcium-dependent signaling. Ten genes encode the core $Ca_V\alpha_1$ subunits. Auxiliary $Ca_V\beta$ and $Ca_V\alpha_2\delta$ subunits and additional associated proteins modulate surface expression efficiency, subcellular targeting, biophysical properties, and pharmacology of the $Ca_V\alpha_1$ subunit (Birnbaumer et al. 1998; Helton et al. 2002; Hering 2002; Walker and De Waard 1998).

Alternative splicing of $Ca_V\alpha_1$ pre-mRNAs is extensive, endowing individual $Ca_V\alpha_1$ genes with the capacity to generate multiple functionally specialized proteins (Lipscombe et al. 2002). The mammalian nervous system in particular uses alternative splicing to produce an array of functionally distinct and finely tuned proteins (Black 2000; Grabowski 1998). Sites of regulated alternative splicing occur in key functional domains of proteins (Garcia et al. 2004). The IVS3-IVS4 domain of $Ca_V\alpha_1$ is a conserved site of alternative splicing. It is found in multiple Ca_v genes and different species from *Drosophila* to human (Barry et al. 1995; Bourinet et al. 1999; Hans et al. 1999; Ihara et al. 1995; Ligon et al. 1998; Lin et al. 1997, 1999; Lipscombe et al. 2002; Peixoto et al. 1997; Perez-Reyes et al. 1990; Smith et al. 1996, 1998; Snutch et al. 1991; Starr et al. 1991; Takimoto et al. 1997). Splice isoforms with different IVS3-IVS4 linkers can open at different rates and at different voltages and have different drug sensitivities (Bourinet et al. 1999; Hans et al. 1999; Krovetz et al. 2000; Lin et al. 1997, 1999; Lipscombe and Castiglioni 2004). The expression of exons in the IVS3-IVS4 region of at least two genes, $Ca_V1.3$ and $Ca_V2.2$, depends on tissue type (Lin et al. 1999; Takimoto et al. 1997). Evolutionary conservation, modification of channel function, and tissue-specific expression combine to suggest that alternative splicing in the IVS3-IVS4 region of $Ca_V\alpha$ is physiologically important.

In the $Ca_V2.2$ gene, exon 24a (e24a) encodes a tetrapeptide sequence, SFMG, in domain IIIS3-IIIS4 and exon 31a (e31a), the dipeptide sequence ET in domain IVS3-IVS4 (Lipscombe et al. 2002). The expression pattern of these exons differs. In sympathetic neurons, all $Ca_V2.2$ mRNAs contain e31a, whereas this exon is absent in $Ca_V2.2$ mRNAs of brain and spinal cord. Exon e24a is present in an approximate reciprocal distribution. Most $Ca_V2.2$ mRNAs in brain and spinal cord contain e24a, whereas in sympathetic and dorsal ganglia a slight majority lack e24a (Lin et al. 1997). In previous studies, we characterized some aspects of alternative splicing in the S3–S4 linkers of the $Ca_V2.2$ channel in the *Xenopus* oocyte expression system. Our functional analyses in *Xenopus* oocytes showed that the peripheral-dominant $Ca_V2.2e[\Delta 24a, 31a]$ splice form activated more slowly and at voltages slightly more depolarized compared with the central-dominant form, $Ca_V2.2e[24a, \Delta 31a]$ (Lin et al. 1997, 1999). Subsequently, we showed that the presence of e31a in domain IVS3-IVS4 accounts fully for the slower activation time course of the $Ca_V2.2e[\Delta 24a, 31a]$ splice isoform, whereas both e24a and e31a contributed to the difference in activation thresholds (Lin et al. 1999).

In the present study, we generate mammalian cell lines (tsA201) stably expressing the N-type $Ca_V2.2$ splice forms

* All authors contributed equally to this work.

Address for reprint requests and other correspondence: D. Lipscombe, Dept. of Neuroscience, Brown University, 192 Thayer St., Providence, RI 02912 (E-mail: Diane_Lipscombe@Brown.Edu).

The costs of publication of this article were defrayed in part by the payment of page charges. The article must therefore be hereby marked "*advertisement*" in accordance with 18 U.S.C. Section 1734 solely to indicate this fact.

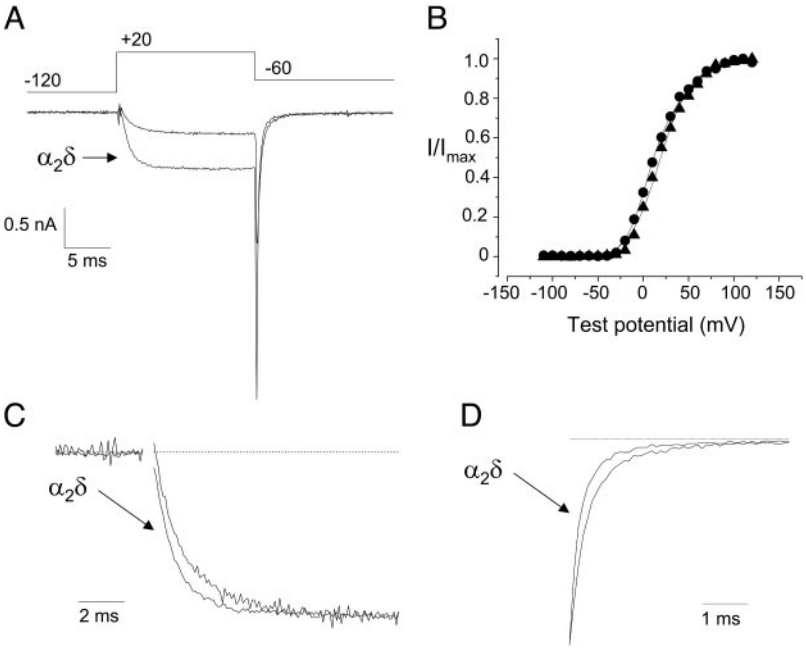

FIG. 1. $Ca_V\alpha_2\delta$ speeds N-type channel activation and deactivation. *A*: N-type channel currents recorded in tsA201 cells expressing $Ca_V2.2$e[24a, Δ31a], $Ca_V\beta_3$ with (●) and without (▲) exogenous $Ca_V\alpha_2\delta_1$. Activation and deactivation time courses are shown on an expanded time scale in *C* and *D* normalized to peak inward currents or peak tail currents. Average macroscopic activation and deactivation time constants from currents expressed with and without $Ca_V\alpha_2\delta_1$ are compared in Table 1. *B*: voltage dependence of channel opening measured with tail current activation curves from the same cells shown in *A*. Currents with $Ca_V\alpha_2\delta_1$ were fit with the sum of 2 Boltzmann functions and without $Ca_V\alpha_2\delta_1$ with a single Boltzmann. Values with $Ca_V\alpha_2\delta_1$: $V_{1/2\text{-}1} = 1.4$ mV and $k_1 = 10.6$ mV, $V_{1/2\text{-}2} = 39.6$ mV, and $k_2 = 18.4$ mV; without $Ca_V\alpha_2\delta_1$: $V_{1/2} = 12.4$ mV and $k = 16.8$ mV. Average $V_{1/2}$ and k values are shown in Table 1. Current amplitudes between splice forms were not significantly different regardless of whether $Ca_V\alpha_2\delta_1$ was co-expressed. Peak tail currents with $Ca_V\alpha_2\delta_1$ measured 9.5 ± 1.1 nA for $Ca_V2.2$ e[24a, Δ31a] ($n = 22$) and 10.9 ± 1.1 nA for $Ca_V2.2$ e[Δ24a, 31a] ($n = 28$). Peak tail currents without $Ca_V\alpha_2\delta_1$ measured 1.4 ± 0.3 nA for $Ca_V2.2$ e[24a, Δ31a] ($n = 6$) and 1.0 ± 0.1 nA for $Ca_V2.2$ e[Δ24a, 31a] ($n = 5$).

with $Ca_V\beta_3$ alone or $Ca_V\beta_3$ and $Ca_V\alpha_2\delta$, the full complement of auxiliary subunits. We show that the presence of $Ca_V\alpha_2\delta$ is necessary to reconstitute native-like ionic currents and confirm that $Ca_V2.2$ splice isoforms activate at different rates but find no difference in ionic activation thresholds as reported in previous studies using the oocyte expression system. Gating currents measured from heterologously expressed $Ca_V2.2$ splice forms decay with significantly different rates, but activation thresholds of gating currents are identical. Our analysis of ionic and gating currents in these stable cell lines correlates with native currents recorded from sympathetic and hippocampal pyramidal neurons. Our findings support the conclusion that alternative splicing in the S3-S4 linkers of $Ca_V2.2$ primarily serves to modify channel gating kinetics.

Note on nomenclature

In this paper, we use $Ca_V2.2$ for the alpha1 subunit of the N-type calcium channel (Ertel et al. 2000). There is no accepted nomenclature to identify splice isoforms. We know the structure of the human $Ca_V2.2$ gene (Lipscombe et al. 2002) and therefore use specific exon numbers to distinguish splice isoforms. The SFMG splice site in domain IIIS3-IIIS4 of $Ca_V2.2$ is encoded by exon 24a and the ET site in domain IVS3-IVS4 by exon 31a. The peripheral-dominant splice isoform studied here is $Ca_V2.2$ e[Δ24a, 31a], formerly named rn$\alpha_{1B\text{-}a}$, and the central-dominant splice isoform is $Ca_V2.2$ e[24a, Δ31a], formerly rn$\alpha_{1B\text{-}c}$ (Lin et al. 1997).

METHODS

Establishing stable lines

We generated four tsA201 cell lines that stably express the following calcium channel subunits. *1*) $Ca_V2.2$ e[Δ24a, 31a] and $Ca_V\beta_3$; *2*) $Ca_V2.2$ e[24a, Δ31a] and $Ca_V\beta_3$; *3*) $Ca_V2.2$ e[Δ24a, 31a], $Ca_V\beta_3$, and $Ca_V\alpha_2\delta_1$; and *4*) $Ca_V2.2$ e[24a, Δ31a], $Ca_V\beta_3$, and $Ca_V\alpha_2\delta_1$. All clones were generated in our laboratory. $Ca_V2.2$ subunits were subcloned into pcDNA6, blasticidin selection (Invitrogen). The two clones $Ca_V2.2$ e[Δ24a, 31a] and $Ca_V2.2$ e[24a, Δ31a], originally called rn$\alpha_{1B\text{-}a}$ and rn$\alpha_{1B\text{-}c}$ (Lin et al. 1997) (GenBank No. AF055477), were linearized with *Spe*I. $Ca_V\beta_3$ was PCR-amplified from rat brain (Pan and Lipscombe 2000), subcloned into pcDNA3.1 (zeocin), and linearized by *Pvu*I. $Ca_V\alpha_2\delta_1$ was isolated from a rat superior cervical ganglia cDNA library (GenBank No. AF286488), subcloned into pcDNA3 (hygromycin), and linearized with *Spe*I. (see http://neuroscience.brown.edu/LipscombeLab/HOMEPAGE/home2.htm for additional information on clones).

TABLE 1. *Activation kinetics*

	$\tau_{activation}$, ms	$\tau_{deactivation}$, ms	τ_{gate}, ms	Gating $V_{1/2}$, mV	Gating k, mV	Ionic $V1_{1/2}$, mV	Ionic k1, mV	Ionic $V2_{1/2}$, mV	Ionic k2, mV
$Ca_V\alpha_2\delta$									
[24a, Δ31a]	0.69 ± 0.02 (12)	0.26 ± 0.01 (6)	0.16 ± 0.02 (9)	−44.7 ± 2.2 (8)	9.0 ± 1.0 (8)	−3.7 ± 2.1 (7)	8.5 ± 0.4 (7)	48.6 ± 2.4 (7)	16.7 ± 1.2 (7)
[Δ24a, 31a]	1.17 ± 0.07 (16)	0.35 ± 0.03 (5)	0.28 ± 0.02 (10)	−39.5 ± 2.5 (10)	10.8 ± 1.2 (10)	−0.6 ± 1.6 (10)	7.5 ± 0.5 (10)	42.2 ± 4.0 (8)	16.8 ± 1.1 (8)
w/o $Ca_v\alpha_2\delta$									
[24a, Δ31a]	1.63 ± 0.13 (6)	0.33 ± 0.03 (6)				17.2 ± 2.3 (6)	16.7 ± 0.7 (6)		
[Δ24a, 31a]	2.47 ± 0.36 (4)	0.54 ± 0.03 (5)				12.9 ± 2.6 (5)	15.5 ± 0.9 (5)		
Native N-type									
Pyramidal*	1.22 ± 0.1 (7)	0.26 ± 0.01 (8)				2.5 ± 1.3 (7)	5.4 ± 0.2 (7)		
Sympathetic*	1.67 ± 0.08 (6)	0.33 ± 0.02 (6)				4.6 ± 1.8 (6)	4.6 ± 0.2 (6)		

For clones, activation kinetics measured at 0 mV, deactivation kinetics at −60 mV with 2 Ba. Values are means ± SE. Numbers of neurons are in parentheses. For comparison, in *Xenopus* oocytes, activation kinetics for [24a, Δ31a] and [Δ24a, 31a] were 2 ms and 4.5 ms at +10 mV with 5 Ba (Lin et al. 1997). *For native N-type, activation kinetics measured at +10 mV and deactivation kinetics measured at −50 mV with 5 Ba.

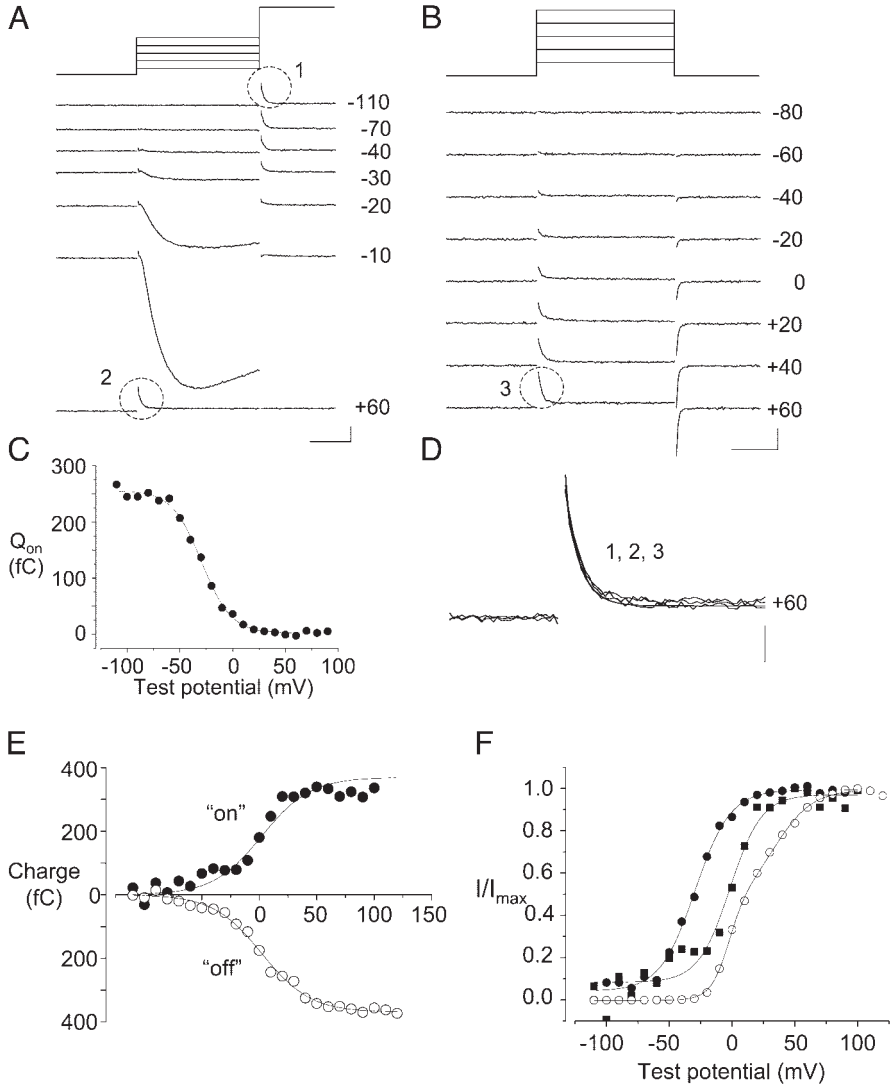

FIG. 2. Comparison of gating currents measured in barium and with ionic currents blocked by cobalt and cadmium. All data were taken from the same tsA 201 cell expressing $Ca_V2.2$e[Δ24a, 31a], $Ca_V\beta_3$, and $Ca_V\alpha_2\delta_1$. *A*: a series of traces showing gating currents at +60 mV, determined to be the ionic reversal potential in this cell. Step depolarizations indicated were applied from a holding potential of –120 mV before stepping to +60 mV. The decrease in the ON gating current at +60 mV as a function of the preceding test voltage is shown in *C*. Currents were recorded in 2 mM barium and are shown leak subtracted. Scale bars: 0.5 nA, 5 ms. *B*: a series of traces showing ON and OFF gating currents recorded in the presence of 2 mM cobalt and 0.2 mM cadmium. Currents were activated by test depolarizations as indicated from a holding potential of –120 mV. Currents shown are leak subtracted. Scale bars: 0.4 nA, 5 ms. *C*: total charge movement during ON gating currents measured at +60 mV as a function of the preceding depolarization. The Boltzmann fit to the data has values $V_{1/2} = -29.4$ mV and $k = 13.9$ mV. *D*: gating currents measured at +60 mV shown on an expanded time base taken from recordings indicated by circles (1–3) in *A* and *B*. Three traces are superimposed, 2 in the presence of barium (1, 2) and 1 in cobalt and cadmium (3). Gating currents have the same time course. An exponential fit ($\tau = 0.36$ ms) to the current recorded in cobalt and cadmium (3) is superimposed. Scale bars: 0.2 nA, 2 ms. *E*: relationship between total charge moved and test voltage for ON and OFF gating currents in *B* measured in the presence of cobalt and cadmium. The total charge of ON and OFF gating currents is the same. The Boltzmann fit to the OFF gating current relationship is superimposed on OFF data points and the same fit, inverted, on ON data points. $V_{1/2} = 2.2$ mV and $k = 20.9$ mV. *F*: activation curves for gating currents in barium (full circle), gating currents in cobalt and cadmium (full square), and ionic tail currents in barium (open circle). Single Boltzmann functions were fit to gating activation curves and are shown superimposed on the data. $V_{1/2}$ and k values in barium: $V_{1/2} = -29.4$ mV and $k = 13.9$ mV; and in cobalt and cadmium: $V_{1/2} = -1.7$ mV and $k = 12.5$ mV. Activation curves for ionic tail currents were fit with the sum of 2 Boltzmann functions: $V_{1/2\text{-}1} = -2.6$ mV and $k_1 = 7.1$ mV, $V_{1/2\text{-}2} = 34.9$ mV and $k_2 = 14.7$ mV

Two cell lines were initially generated that stably expressed one of the two $Ca_V2.2$ splice forms together with $Ca_V\beta_3$. tsA201 cells were transfected by electroporation with a 10 μg mix of linearized $Ca_V2.2$ and $Ca_V\beta_3$ cDNAs. Cells were diluted and grown without antibiotics for 2 days; 7.5 μg/ml blasticidin and 250 μg/ml zeocin were then added and single colonies isolated 10 days later. Selection with blasticidin and zeocin was very efficient. For example, 20 of 20 colonies contained $Ca_V2.2$ e[Δ24a, 31a] and 18 of 20 contained $Ca_V\beta_3$ based on PCR screening. For each condition, six cell lines were chosen randomly for functional screening by whole cell recording, and two cell lines that contained high current density were selected. There was significant variability in current density among cells in each line. A second round of dilution cloning, PCR screening, and functional assessment was carried out, and 20 new colonies were isolated for each subunit combination. Cell lines 2017 ($Ca_V2.2$ e[Δ24a, 31a], $Ca_V\beta_3$) and 1911 ($Ca_V2.2$ e[24a, Δ31a], $Ca_V\beta_3$) were selected for further study because they had particularly high current density and homogenous expression levels among cells. Cells were maintained in DMEM supplemented with 10% fetal bovine serum, 5 μg/ml blasticidin, and 250 μg/ml zeocin. Expression levels of the two splice forms were approximately equal as measured by current density. Peak current densities were -31.2 ± 4.4 (SE) pA/pF ($n = 9$) and -28.1 ± 6.6 pA/pF ($n = 9$) for $Ca_V2.2$ e[Δ24a, 31a] and $Ca_V2.2$ e[24a, Δ31a], respectively. Lines 2017 and 1911 were then used to generate $Ca_V\alpha_2\delta_1$-expressing cells as described in the preceding text. After a further round of dilution cloning, lines 201719 ($Ca_V2.2$ e[Δ24a, 31a], $Ca_V\beta_3$, $Ca_V\alpha_2\delta_1$) and 191105 ($Ca_V2.2$ e[24a, Δ31a], $Ca_V\beta_3$, $Ca_V\alpha_2\delta_1$) were used for further study. We fully sequenced all $Ca_V2.2$ cDNAs from these cell lines to ensure that no random mutations were introduced.

Recording methods

All recordings were carried out at room temperature (22–23.5°C). Currents were recorded using the whole cell recording method (Axopatch 200A), digitized at 10 kHz, and low-pass filtered at frequencies between 2 and 5 kHz. Analysis was performed with pCLAMP7 (Axon Instruments), software was custom-written in Quick Basic or MatLab, and Origin (Microcal). The bath solution contained (in mM) 160 TEA-Cl, 10 HEPES, and 2 $BaCl_2$, pH 7.4 with TEA-OH. The pipette solution contained (in mM) 56 CsCl, 68 CsF, 2.2 $MgCl_2$, 4.5 EGTA, 9 HEPES, 4 MgATP, 14 creatine phosphate (Tris salt), and 0.3 GTP (Tris salt), pH 7.4 with CsOH. Electrode resistances were 1–2 MΩ when filled with pipette solution. The series resistance was always <10 MΩ and compensated ≥90%. Currents evoked by voltage steps were subtracted for leak and capacitance using appropriately scaled currents evoked by a hyperpolarization from the holding potential. ω-conotoxin GVIA (Peptides International or Bachem) was used to isolated N-type currents from whole cell calcium currents in sympathetic and hippocampal neurons.

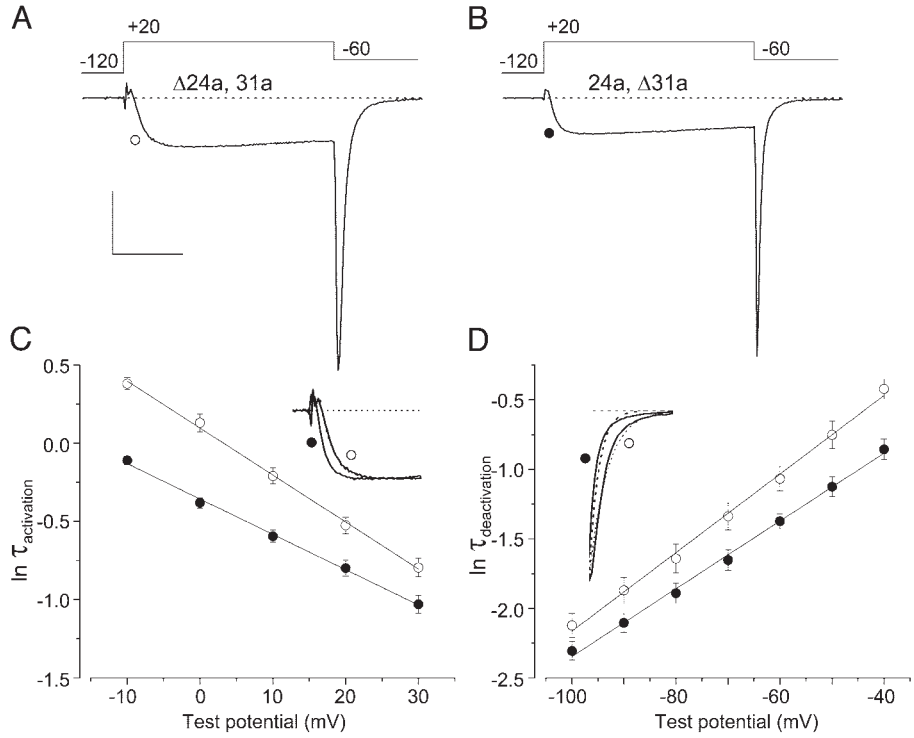

FIG. 3. $Ca_V2.2e[\Delta 24a, 31a]$ splice form activates and deactivates slower than $Ca_V2.2e[24a, \Delta 31a]$. Calcium channel currents were recorded from tsA201 cells stably expressing $Ca_V2.2e[\Delta 24a, 31a]$ (○) and $Ca_V2.2e[24a, \Delta 31a]$ (●), together with $Ca_V\beta_3$ and $Ca_V\alpha_2\delta_1$. *A* and *B*: currents from exemplar cells activated by test depolarizations to +20 mV from a holding potential of –120 mV. Tail currents were recorded by repolarizing to –60 mV. Scale bar: 2 nA, 5 ms. *C*: average macroscopic activation time constants (natural log scale) as a function of test potential for $Ca_V2.2e[\Delta 24a, 31a]$ (○, $n = 16$) and $Ca_V2.2e[24a, \Delta 31a]$ (●, $n = 12$). *Inset*: the exemplar test currents from *A* and *B* normalized to peak inward current to show the slower activation of $Ca_V2.2e[\Delta 24a, 31a]$ with superimposed single exponential fits ($\cdots$). Average time constants for $Ca_V2.2e[\Delta 24a, 31a]$ and $Ca_V2.2e[24a, \Delta 31a]$ were significantly different at all voltages ($P < 0.05$). Lines are best fit linear regressions for $Ca_V2.2e[\Delta 24a, 31a]$: slope = -0.026 ± 0.001 mV^{-1} and y intercept = 0.03 ± 0.05 ms; for $Ca_V2.2e[24a, \Delta 31a]$: slope = -0.021 ± 0.004 mV^{-1} and y intercept = -0.36 ± 0.03 ms. Slopes and intercepts are each significantly different ($P < 0.05$). *D*: average macroscopic deactivation time constants for each splice form (natural log scale) as a function of repolarization potential. *Inset*: the exemplar repolarization currents from *A* and *B* normalized to peak tail current amplitude, to show the slower deactivation of $Ca_V2.2e[\Delta 24a, 31a]$, with superimposed exponential fits. Average time constants were significantly different between splice isoforms at −80, −70, −60, −50, and −40 mV ($P < 0.05$) but were not significantly different at −100 and −90 mV ($P > 0.05$). Lines are best-fit linear regressions: for $Ca_V2.2e[\Delta 24a, 31a]$: slope = 0.028 ± 0.002 and y intercept = 0.66 ± 0.10, $n = 5$; for $Ca_V2.2e[24a, \Delta 31a]$: slope = 0.024 ± 0.001 mV^{-1} and y intercept = 0.09 ± 0.10, $n = 6$. Slopes and intercepts are each significantly different ($P < 0.05$). Values plotted are means ± SE.

Except as noted, statistics are given as means ± SE and significance was tested by unpaired Student's *t*-test.

Gating currents

Gating currents were resolved in cells expressing $Ca_V2.2$ together with $Ca_V\beta_3$ and $Ca_V\alpha_2\delta$. Currents were sampled at 10 kHz and filtered at 5 kHz; twice the digitization frequency to avoid aliasing. At 5 kHz (−3 dB), the rise time of events is 66.42 μs. For event amplitudes to be measured reliably, durations should be at least two times t_r or 132 μs (Colquhoun 1994). It is possible that our fastest signals (160 μs for ON gating of central dominant isoform) were slightly undersampled and amplitudes underestimated. However, these were clearly distinguishable from the slower gating currents of the peripheral dominant isoform (τ = 280 μs) that were well resolved. Nonlinear charge movements were recorded in barium with steps directly to the ionic reversal potential. The reversal potential was determined for each cell and was between +55 and +65 mV. Currents were induced by step depolarizations from a holding potential of between –100 and –120 mV. Leak subtraction was carried out off-line with appropriately scaled currents evoked by a 10 or 20 mV hyperpolarization from the holding potential. Recordings were only made from cells with small leak currents, in the range of 10–50 pA at the holding potential (−100 or –120 mV). Small transient outward currents remained after leak subtraction of size in relation to ionic currents appropriate for gating currents (Jones et al. 1997–1999; Noceti et al. 1996). No nonlinear charge movements were recorded from cells expressing no or very few functional channels. Similar nonlinear charge movements were recorded at the onset and offset of test depolarizations when ionic currents were blocked by replacing 2 mM Ba^{2+} with 2 mM Co^{2+} and 0.2 mM Cd^{2+}.

RESULTS

$Ca_V\alpha_2\delta$ subunit modifies channel gating kinetics

N-type Ca channel currents were recorded from mammalian tsA201 cells stably expressing $Ca_V2.2e[24a, \Delta 31a]$ together with $Ca_V\beta_3$ and $Ca_V\alpha_2\delta_1$ (Fig. 1). For both splice forms, gating kinetics of the channels in tsA201 cells were significantly faster than those of the same clones expressed in *Xenopus* oocytes with $Ca_V\beta_3$ (Lin et al. 1997) and resembled N-type currents of neurons (see following text; Table 1). At least part of the explanation for faster and more native-like gating kinetics of $Ca_V2.2$ clones in tsA201 cells is the presence of exogenous $Ca_V\alpha_2\delta_1$ (Fig. 1). The $Ca_V\alpha_2\delta_1$ auxiliary subunit was

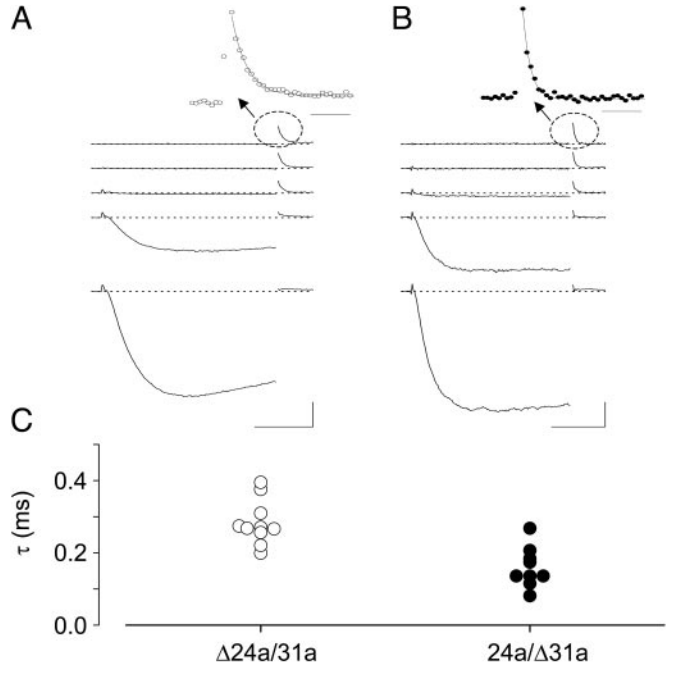

FIG. 4. Slower movement of gating charge recorded from the $Ca_V2.2e[\Delta 24a, 31a]$ splice isoform. *A* and *B*: currents recorded from exemplar cells expressing $Ca_V2.2e[\Delta 24a, 31a]$, $Ca_V\beta_3$, and $Ca_V\alpha_2\delta_1$ (○; *A*) and $Ca_V2.2e[24a, \Delta 31a]$, $Ca_V\beta_3$, and $Ca_V\alpha_2\delta_1$ (●; *B*). Cells were held at –120 mV and currents were activated by a family of test depolarizations, each followed by a step to the ionic reversal potential. At the ionic reversal potential, the only current flowing is transient outward current from ON gating charge movement. Currents shown are in response to test pulses to, from top to bottom, −110, −70, −40, −20, and −10 mV. Test pulses to successively stronger depolarizations left successively less gating charge to be moved by the subsequent step to the ionic reversal potential. For the cells shown, the ionic reversal potential was +60 mV for $Ca_V2.2e[\Delta 24a, 31a]$ and +62 mV for $Ca_V2.2e[24a, \Delta 31a]$. *Inset*: the circled area shown at expanded scale. Single-exponential fits, representing the speed of ON charge movement, are superimposed on the decay phase of the ON gating current. Fitted time constants were 0.38 ms (*left*) and 0.18 ms (*right*). Scale bars: 5 ms, 1 nA. All currents were leak-subtracted off-line with scaled currents evoked by a pulse from –120 to –130 mV. *C*: gating current decay time constants for all cells recorded with this protocol. Each point shows time constant of decay of ON gating current from a single cell. Each point is the average of the time constants of ON gating current decay measured at the reversal potential following pulses to −110 and −100 mV. Average values: $Ca_V2.2e[\Delta 24a, 31a]$ = 0.28 ms ± 0.02 ms (n = 10 cells); $Ca_V2.2e[24a, \Delta 31a]$ = 0.16 ms ± 0.02 ms (n = 9 cells). These values are significantly different ($P < 0.05$).

not included in our earlier studies of the same clones in *Xenopus* oocytes, although it is known to be part of the in vivo N-type channel complex (Witcher et al. 1993) and to speed N-type channel gating kinetics in oocytes (Wakamori et al. 1999). Another factor could be species-dependent posttranslational modifications between the two expression systems. To test this, currents were recorded from tsA201 cell lines expressing the same subunit combination used in our earlier oocyte studies: $Ca_V2.2$ splice form together with $Ca_V\beta_3$ without exogenous $Ca_V\alpha_2\delta_1$. Current densities were significantly smaller in the absence of exogenous $Ca_V\alpha_2\delta_1$ (Fig. 1, legend). N-type currents in tsA201 cells without exogenous $Ca_V\alpha_2\delta_1$ activate and deactivate significantly more slowly than those with exogenous $Ca_V\alpha_2\delta_1$ (Fig. 1, *C* and *D;* Table 1), more like currents recorded in oocytes. Macroscopic $Ca_V2.2e[24a, \Delta 31a]$ currents activated with time constants of ~2 ms at +10 mV in *Xenopus* oocytes (Lin et al. 1997), compared with 1.6 and 0.7 ms in tsA201 cells in the absence and presence of $Ca_V\alpha_2\delta_1$, respectively (Table 1). Activation curves generated from tail current analysis in cells expressing exogenous $Ca_V\alpha_2\delta_1$ were also steeper at voltages between −30 and +30 mV compared with those generated from cells lacking $Ca_V\alpha_2\delta_1$ and generally contained two Boltzmann components rather than one (Figs. 1*B*, 2*F*, and 5*A*). We conclude that the presence of $Ca_V\alpha_2\delta_1$ is an important determinant of channel kinetics, accounting for the faster, more native-like kinetics of currents in tsA201 cells that express exogenous $Ca_V\alpha_2\delta_1$.

Gating current measurements

Current densities and therefore channel expression levels were sufficiently high in these stable cell lines to resolve gating charge movement: about nine elementary charges per channel (Noceti et al. 1996). We recorded gating currents using identical ionic conditions as those used to record ionic currents (Figs. 2, 4, and 5). We applied test pulse depolarizations to precisely the ionic reversal potential where net current is zero. After leak subtraction only small, transient currents remained that decayed with time constants in the range of 0.2–0.3 ms, consistent with the time course of ON gating currents (Fig. 2, *A*, *B*, and *D*) (Jones et al. 1997, 1999; Noceti et al. 1996). Figure 2 shows that the kinetics of these gating currents were the same when measured in barium at the ionic reversal potential (+60 mV) and when measured in the same cell with ionic currents blocked by a combination of cobalt (2 mM) and cadmium (0.2 mM) (compare Fig. 2, *A* and *B*, and see *D*). The time course of the gating current during the test pulse, representing the speed of ON movement of the charge sensor, was fit well by a single exponential function (τ = 0.36 ms for this cell expressing $Ca_V2.2e[\Delta 24a, 31a]$; Fig. 2*D*). As a control, we also show that the total charge during ON gating currents equals that of OFF gating currents, over a range of potentials (Fig. 2, *B* and *E*). The size of ON gating currents at the reversal potential diminished as the magnitude of the prepulse depolarization immediately preceding the step to +60 mV was increased (Fig. 2, *A* and *C*). This is expected for current originating from the movement of putative voltage sensors. As progressively more channels activate and as more gating charge moves during the prepulse, a proportionally smaller number of channels is available for activation and less gating charge moves during the subsequent test pulse. The total charge left to move at +60 mV as a function of prepulse voltage is shown in Fig. 2*C*. The inverse of this plot is the ON gating current activation curve (Figs. 2*F* and 5*B*). As expected, gating currents activate at voltages more hyperpolarized than those that elicit ionic currents (~40 mV; Figs. 2*F*, and 5, *C* and *D*, also see Table 1). However, we found that gating currents in the presence of cobalt and cadmium required much stronger depolarizations to activate (~25 mV more depolarized) compared with those recorded in barium (Fig. 2*F*). Differences in surface charge screening between barium and cobalt may account for the differential shifts in the voltage dependence of channel gating (Hille et al. 1975). To avoid the need to correct for surface charge screening and to facilitate direct comparisons between gating and ionic currents, we measured gating currents at the ionic reversal potential in the presence of 2 mM barium.

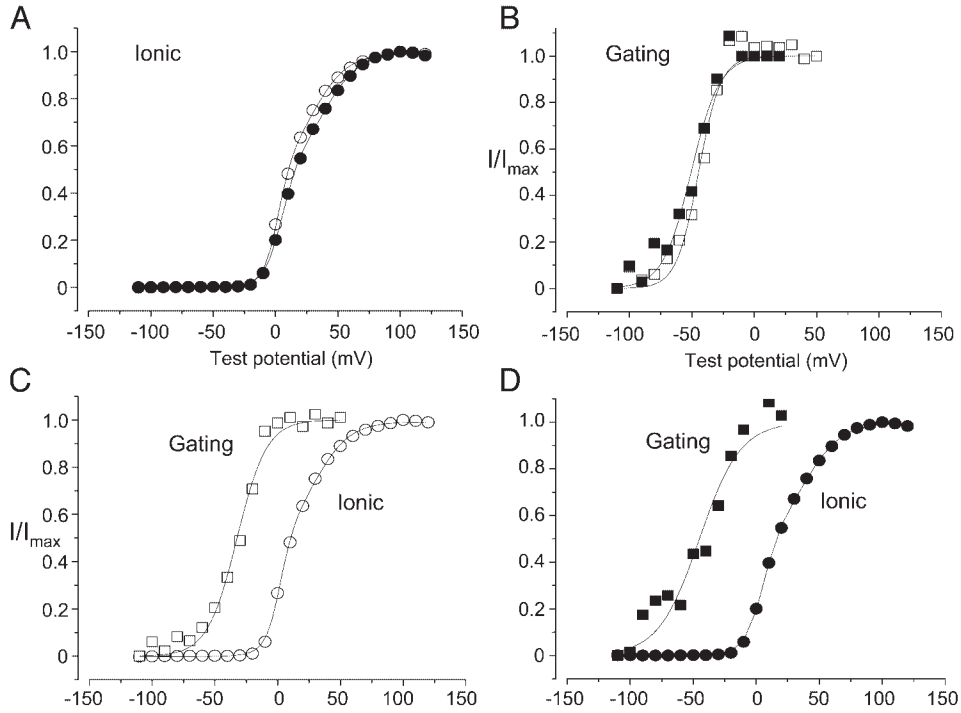

FIG. 5. Alternative splicing in S3-S4 does not affect the steady-state voltage dependence of channel opening or of gating charge movement. Comparison of activation curves for channel opening (*A*, ○, ●) and gating charge movement (*B*, □, ■) in representative cells expressing $Ca_V2.2e[\Delta 24a, 31a]$ (□, ○) and $Ca_V2.2e[24a, \Delta 31a]$ (■, ●). Currents are normalized to peak. Voltage dependence of charge movement was measured with the protocol of Fig. 2. Fractional gating charge movement as a function of voltage (*B–D*) was obtained by integrating the ON currents in barium at the reversal potential as a function of prepulse voltage (e.g., Fig. 2, *A* and *C*), normalizing total charge moved to the maximum, and subtracting each value from 1 to display data as the fraction of charge moved rather than the fraction of charge not moved. The voltage dependence of channel opening reflects tail current activation curves assayed by replacing the step to the ionic reversal potential with a repolarization to −60 mV. Activation curves for gating charge movement are fit by single Boltzmann functions. Activation curves for channel opening are fit by the sum of 2 Boltzmann functions. Curves shown are Boltzmann fits to individual data sets. $V_{1/2}$ and k values were for *A*, $Ca_V2.2e[\Delta 24a, 31a]$: $V_{1/2\text{-}1} = 2.1$ mV and $k_1 = 5.6$ mV, $V_{1/2\text{-}2} = 30.2$ mV and $k_2 = 13.8$ mV; $Ca_V2.2e[24a, \Delta 31a]$: $V_{1/2\text{-}1} = 5.2$ mV and $k_1 = 7.0$ mV, $V_{1/2\text{-}2} = 40.1$ mV and $k_2 = 14.1$ mV. For *B*, $Ca_V2.2e[\Delta 24a, 31a]$: $V_{1/2} = -46.0$ mV and $k = 9.2$ mV; $Ca_V2.2e[24a, \Delta 31a]$: $V_{1/2} = -50.0$ mV and $k = 11.4$ mV. For *C*, gating: $V_{1/2} = -32.2$ mV and $k = 11.8$ mV; ionic: $V_{1/2\text{-}1} = 2.1$ mV and $k_1 = 5.6$ mV, $V_{1/2\text{-}2} = 30.2$ mV and $k_2 = 13.8$ mV. For *D*, gating: $V_{1/2} = -41.7$ mV and $k = 17.8$ mV; ionic: $V_{1/2\text{-}1} = 5.2$ mV and $k_1 = 7.0$ mV, $V_{1/2\text{-}2} = 40.0$ mV and $k_2 = 14.1$ mV. Average $V_{1/2}$ and k values estimated from fits to all individual data sets are shown in Table 1. There is no significant difference in $V_{1/2}$ and k values between $Ca_V2.2e[\Delta 24a, 31a]$ and $Ca_V2.2e[24a, \Delta 31a]$ for ionic or gating currents.

Alternative splicing in S3-S4 modifies ionic current kinetics

We compared N-type currents recorded from tsA201 cells stably expressing each $Ca_V2.2$ splice isoform. Macroscopic $Ca_V2.2e[\Delta 24a, 31a]$ currents activated and deactivated with time constants that were significantly longer compared with $Ca_V2.2e[24a, \Delta 31a]$ (Fig. 3, *C* and *D*; $P < 0.05$; Table 1). That is, the predicted peripheral-dominant clone activated and deactivated more slowly than the predicted central-dominant clone. The difference in activation speed was ~1.5-fold over a range of voltages. This difference in macroscopic activation kinetics was also independent of the presence of $Ca_V\alpha_2\delta_1$ (Table 1) and matches almost exactly our previous studies of the same splice isoforms in *Xenopus* oocytes (Lin et al. 1997, 1999).

Gating currents of S3-S4 splice forms decay at different rates

We compared gating currents from cells expressing $Ca_V2.2$ splice isoforms as described earlier. Gating currents measured in cells expressing $Ca_V2.2$ e[Δ24a, 31a] decayed with time courses that were significantly slower (1.7-fold) compared with $Ca_V2.2$ e[24a, Δ31a] ($P < 0.05$; Fig. 4; Table 1). The 1.7-fold difference parallels the different gating kinetics of ionic currents between splice forms (Figs. 3*C*; Table 1). Although gating currents were measured at +60 mV, ionic currents were measured at voltages between −10 and +30 mV. Our results suggest that alternative splicing in IVS3-IVS4 linker in $Ca_V2.2$ modifies the rate of movement of the voltage sensor that precedes channel opening.

Steady-state voltage dependence of activation does not differ between isoforms

Next we analyzed the steady-state voltage dependence of activation of ionic and gating currents. In our previous studies, we reported a small (~7 mV) but significant difference in the voltage dependence of channel activation between splice isoforms expressed in oocytes. This difference was not recapitulated in mammalian cells (Table 1; Fig. 5*A*). Most ionic current activation curves (8 of 10 recordings) were best fit by two Boltzmann functions with activation mid-points close to 0 and +45 mV, respectively (Figs. 2*F* and 5*A*; Table 1). There was no consistent difference in tail current activation curves between splice isoforms. In contrast to ionic currents, activation curves of gating

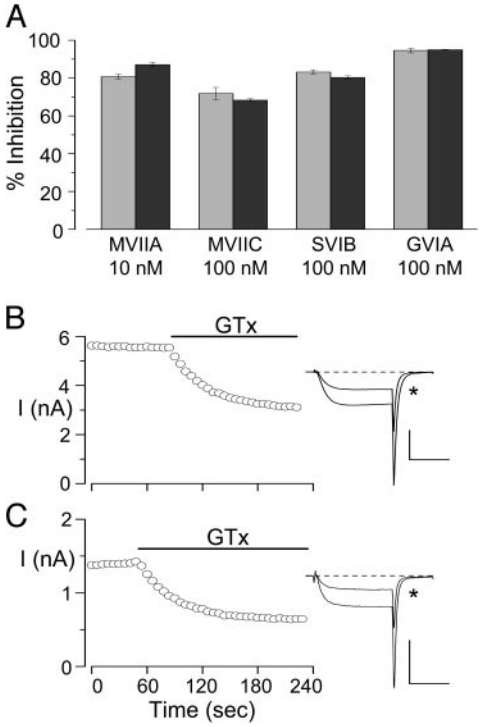

FIG. 6. Alternative splicing in the voltage sensor does not affect fractional inhibition by peptide toxins that inhibit N-type channels. *A*: histogram compares the degree of inhibition of $Ca_V2.2e[24a, \Delta31a]$ (■) and $Ca_V2.2e[\Delta24a, 31a]$ (□) currents by ω-CTx-MVIIA: $Ca_V2.2e[24a, \Delta31a]$, 87%, $n = 3$; $Ca_V2.2e[\Delta24a, 31a]$, 81%, $n = 4$. ω-CTx-MVIIC: $Ca_V2.2e[24a, \Delta31a]$, 68%, $n = 4$; $Ca_V2.2e[\Delta24a, 31a]$, 72%, $n = 4$. SVIB: $Ca_V2.2e[24a, \Delta31a]$, 80%, $n = 3$; $Ca_V2.2e[\Delta24a, 31a]$, 83%, $n = 4$. ω-CTx-GVIA: $Ca_V2.2e[24a, \Delta31a]$, 95%, $n = 3$; $Ca_V2.2e[\Delta24a, 31a]$, 95%, $n = 3$. Values are not significantly different ($P > 0.05$ for all values). Currents were evoked by a 40-ms step-pulse to 10 mV from a holding potential of –100 mV. Cells expressed $Ca_v2.2$ splice forms together with $Ca_V\beta_3$. 2 mM calcium used as charge carrier. *B* and *C*: equal inhibition of the 2 splice variants by the gating modifier toxin ω-grammotoxin-SIA. Panels show the time course of inhibition of inward current through $Ca_V2.2e[\Delta24a, 31a]$ (*B*) and $Ca_V2.2e[24a, \Delta31a]$ (*C*) channels by 5 nM GTx. GTx shifted the half-maximal activation voltage of $Ca_V2.2e[\Delta24a, 31a]$ by $+69 \pm 7$ mV ($n = 3$) and of $Ca_V2.2e[24a, \Delta31a]$ by $+88 \pm 1.5$ mV ($n = 4$; toxin-induced shift measured from the 1st of 2 Boltzmann fits in control; data not shown). Each point in the time course represents average inward current evoked by a step to 0 mV (*B*) or +10 mV (*C*) followed by tail currents at –60 mV from a steady holding voltage of –120 mV. For each time course, *inset* shows current trace before and after (*) maximal toxin inhibition. - - -, the 0 current level. Scale bars are 5 nA, 5 ms (*B*) and 2 nA, 5 ms (*C*). Cells expressed $Ca_v2.2$ splice forms together with $Ca_V\beta_3$ and $Ca_V\alpha_2\delta_1$ with 2 mM barium as charge carrier.

currents were well fit by single Boltzmann functions with activation mid-points close to −40 mV (Figs. 2*F* and 5*B*; Table 1). Gating current activation curves were also indistinguishable between splice isoforms (Fig. 5*B;* Table 1; $P > 0.05$ for all parameters). Gating currents activate at voltages ~40 mV more hyperpolarized than those that activate ionic currents (Fig. 5, *C* and *D*, also see Table 1). Interestingly, the gating charge appears to move almost completely before any ionic current is measured, a comparison made possible by recording ionic and gating currents in the same ionic conditions.

Inhibition by peptide toxins

There is considerable interest in pharmacological tools to distinguish between $Ca_V2.2$ splice isoforms in peripheral and central neurons, as potential tools to treat CNS disorders while minimizing blood pressure liability. We tested four *Conus* toxins (GVIA, MVIIA, MVIIC, and SVIB) that are likely pore blockers (McDonough 2004) and found that they inhibited both $Ca_V2.2$ splice isoforms equally well (Fig. 6). We also found equal inhibition by ω-grammotoxin-SIA (GTx), which inhibits inward current by altering the speed and voltage dependence of channel opening (McDonough et al. 1997). Nonetheless, by demonstrating that *Conus* GVIA in particular inhibits both splice isoforms equally well, we used this toxin to isolate and compare native N-type currents from sympathetic and hippocampal neurons.

N-type currents in peripheral and central neurons have different gating kinetics

Several studies have demonstrated biophysical differences between alternatively spliced calcium channel clones studied in heterologous expression systems (Lipscombe et al. 2002), but few connect them to the neurons in which they are expressed. Many factors that affect the behavior of N-type channels including $Ca_V\beta$ subunits and G protein modulation are likely to differ in different types of neurons (Ikeda and Dunlap 1999; Walker and De Waard 1998). However, our analyses of cloned splice isoforms, together with earlier studies reporting tissue-specific expression of alternatively spliced exons in $Ca_V2.2$, make predictions about how native N-type currents in different regions of the nervous system might differ (Lipscombe et al. 2002). The vast majority of N-type currents of sympathetic neurons contain the e31a-containing $Ca_V2.2$ isoform. These N-type currents should activate and deactivate with slower kinetics compared with central neurons that only express $Ca_V2.2$ isoforms lacking e31a. In addition, our analyses in tsA201 cells suggest no significant difference in the voltage-dependence of N-type channel activation between sympathetic (peripheral) and hippocampal (central) neurons.

To compare N-type currents in sympathetic and pyramidal hippocampal neurons, we isolated currents using ω-conotoxin GVIA-subtraction because ω-conotoxin GVIA inhibits both $Ca_V2.2$ splice isoforms equally well. The N-type current represents ~80% of the whole cell calcium channel current in sympathetic neurons and ~20% in hippocampal neurons (Fig. 7). When we compared the voltage dependencies of activation, we found no significant difference between native N-type currents in sympathetic and hippocampal neurons, consistent with our studies in tsA201 cells (Fig. 8, *A* and *B*; Table 1). There was not obvious difference in the time course of inactivation of N-type currents between these cell types, at least during the 20-ms test depolarizations used here (Lin et al. 1999). However, N-type currents isolated from recordings of sympathetic neurons both activated and deactivated with kinetics that were consistently slower than N-type currents recorded from hippocampal neurons (Fig. 8, *C* and *D*; Table 1; $P < 0.05$). In fact, deactivation kinetics of native N-type currents in sympathetic and hippocampal neurons were indistinguishable from $Ca_V2.2$ $e[\Delta24a, 31a]$ and $Ca_V2.2e[24a, \Delta31a]$ splice isoforms expressed in tsA201 cells, respectively (Fig. 7*D;* Table 1). We found that activation kinetics of native N-type currents were somewhat slower than those of $Ca_V2.2$ $e[\Delta24a, 31a]$ expressed in tsA201 cells (Table 1). Although not a perfect match, overall, the time course and voltage depen-

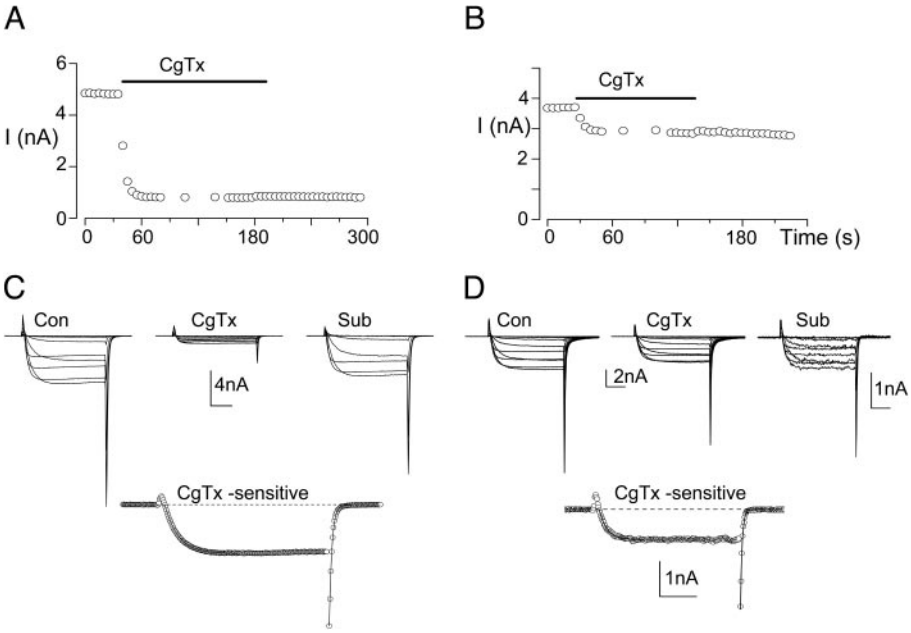

FIG. 7. N-type currents isolated from rat central and peripheral neurons with ω-conotoxin-GVIA. Calcium channel currents were recorded from individual acutely dissociated superior cervical ganglion (*A* and *C*) and hippocampal pyramidal (*B* and *D*) neurons. *A* and *B*: time course of inward calcium channel current amplitude in response to 1 μM ω-CTx-GVIA. Currents were evoked by a depolarization to +20 mV from a holding potential of −70 mV. 1 μM ω-CTx-GVIA inhibited 80% of the total whole cell current in sympathetic neurons and 20% in hippocampal neurons. *C* and *D*: series of calcium channel currents evoked by step depolarizations from –30 to +50 mV at 10-mV increments in control (Con), after inhibition by ω-CgTx-GVIA (CgTx), and toxin-sensitive subtracted currents (Sub). Toxin-sensitive currents on an expanded time scale together with single exponential fits to activation and deactivation kinetics (black lines). Activation and deactivation time constants were 1.6 and 0.31 ms for the sympathetic neuron and 1.1 and 0.24 ms for the pyramidal neuron. Average values are in Table 1. Time bars are 5 ms.

dence of channel opening of native N-type channel currents are most similar to the properties of $Ca_V2.2$ splice isoforms expressed in tsA201 cells that also express $Ca_V\alpha_2\delta_1$ (Figs. 3–5; Table 1). Our results from recordings of cloned and native N-type currents suggest that the major consequence of alternative splicing in the S3-S4 linkers of $Ca_V2.2$ is modulation of channel gating kinetics and not steady-state voltage dependence.

DISCUSSION

We have analyzed the biophysical properties conferred on the N-type channel by two short exons in $Ca_V2.2$ that are differentially expressed in central and peripheral regions of the nervous system (Lin et al. 1997). This form of alternative splicing is characterized by inverse insertions of short cassette exons in domains IIIS3-IIS4 and IVS3-IVS4. Results show that the $Ca_V2.2e[24a, \Delta31a]$ splice isoform gates more rapidly compared with $Ca_V2.2e[\Delta24a, 31a]$ over a range of voltages, independent of expression system and of the presence of the $Ca_V\alpha_2\delta$ auxiliary subunit. Steady-state voltage dependencies of channel opening and of charge movement were not different between splice forms when expressed in mammalian cells. Data from gating currents provide direct evidence that the putative voltage sensor of the $Ca_V2.2e[24a, \Delta31a]$ splice isoform moves faster compared with $Ca_V2.2e[\Delta24a, 31a]$.

Biophysical differences between these splice forms are likely to be physiologically significant because expression of the two exons is under tight cellular control. More generally, alternative splicing, particularly in the IVS3-IVS4 linker, is conserved among $Ca_V\alpha_1$ genes (Lipscombe et al. 2002). In support of this view we show that native N-type currents recorded in hippocampal neurons reflect the faster kinetics of the $Ca_V2.2e[24a, \Delta31a]$ splice isoform, whereas N-type currents in sympathetic neurons consistently gate more slowly similar to $Ca_V2.2e[\Delta24a, 31a]$. Clearly, other factors will contribute to setting the time course of calcium channel activation and deactivation, including G protein activation and association with different $Ca_V\beta$ subunits (Ikeda and Dunlap 1999; Walker and De Waard 1998), and these may differ between sympathetic and hippocampal neurons. $Ca_V2.2$ has been shown to associate with different $Ca_V\beta$ subunits in vivo (Scott et al. 1996). However, we only observed significant differences in activating and deactivation kinetics of native N-type currents in sympathetic and hippocampal neurons consistent with the expression pattern of $Ca_V2.2$ splice isoforms. Exon e31a of $Ca_V2.2$ is particularly notable because it is expressed in peripheral neurons but suppressed throughout the CNS, including the hippocampus. Further, in a previous study we showed that exon 31a can fully confer the slower activation kinetics of the $Ca_V2.2e[\Delta24a, 31a]$ splice isoform (Lin et al. 1999). The different kinetics of ionic and gating currents of $Ca_V2.2$ splice isoforms studied here most likely originate from the splice site in the S3-S4 linker of the fourth domain.

Effects on gating kinetics

The slower gating kinetics of $Ca_V2.2e[\Delta24a, 31a]$ reported here and in earlier studies (Lin et al. 1997, 1999) are consistent with studies of alternative splicing in the equivalent IVS3-IVS4 linker of the closely related $Ca_V2.1$ P/Q-type channel (Hans et al. 1999; Krovetz et al. 2000). The different phenotypes of S3-S4 splice isoforms of $Ca_V\alpha_1$ are interesting in light of the proposed central role this region plays in forming the putative voltage-sensing paddles recently predicted from crystallographic studies of the voltage-gated potassium channel (Jiang et al. 2003; see also Bezanilla 2000; Nakai et al. 1994; Stotz and Zamponi 2001). Apparent rates of activation of macroscopic currents, deactivation rates of macroscopic tail currents, and the speed of ON gating currents all differ between splice forms, with the CNS-dominant $Ca_V2.2e[+24a, \Delta31a]$ channels faster by ~1.5-fold in all cases (Figs. 3 and 4; Table 1). We note, however, that gating currents were monitored at or close to +60 mV, whereas ionic currents were recorded at voltages between –100 and +30 mV where signals are measurable (Fig. 3). Several schemes modeling the kinetics of

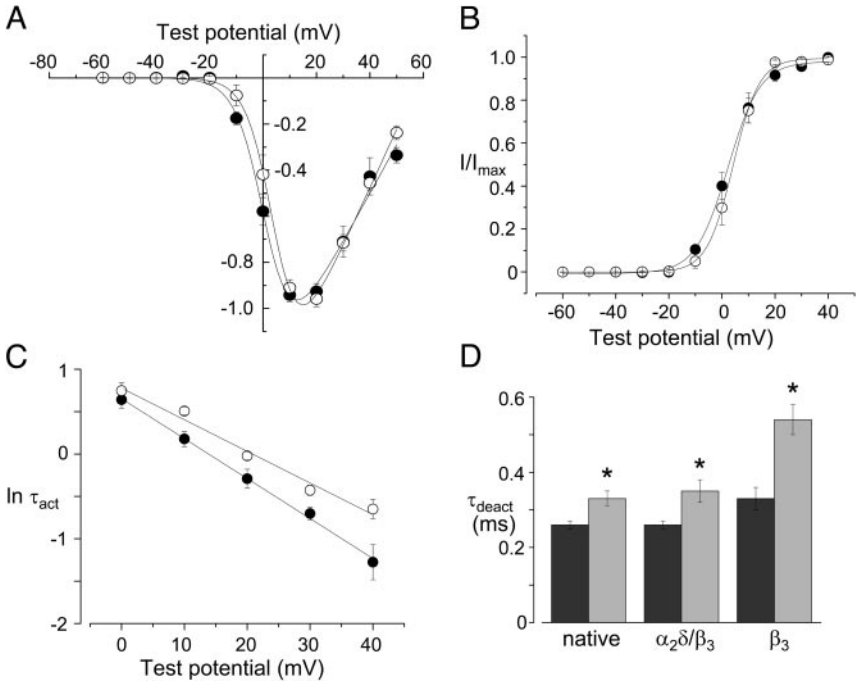

FIG. 8. N-type currents from superior cervical ganglia (SCG) and hippocampal neurons activate and deactivate at different speeds but have the same steady-state voltage dependence of channel opening. Using the protocol of Fig. 4, voltage dependence and kinetics of N-type currents were measured from SCG neurons (○, $n = 6$) and hippocampal pyramidal neurons (●, $n = 7$). Points shown are means ± SE (*A*), voltage dependence of inward N-type currents. Fitted curves are the Boltzmann equation times driving force, $I/I_{max} = 1/\{1 + \exp[(V - V_{1/2})/k]\} * (V - E_{rev})$. Sympathetic neurons: $V_{1/2} = 4.7$ mV, $k = 4.9$ mV; pyramidal neurons: $V_{1/2} = 1.4$ mV, $k = 5.2$ mV. Average values from fits of individual data sets for sympathetic and pyramidal neurons are shown in Table 1. *B*: voltage dependence of fractional current activation estimated from chord conductance with superimposed Boltzmann fits. Average values were calculated from Boltzmann fits to individual data sets. For sympathetic neurons: $V_{1/2} = 4.3 \pm 1.7$ mV, $k = 4.5 \pm 0.1$; for pyramidal neurons: $V_{1/2} = 5.1 \pm 1.8$ mV, $k = 6.4 \pm 0.5$ mV. $V_{1/2}$ values are not significantly different ($P < 0.05$), k values are significantly different ($P > 0.05$). (Note that the curves are right-shifted ~10 mV compared with clones, due to the additional surface charge screening by 5 mM barium compared with 2 mM barium). *C*: macroscopic activation time constants of N-type currents from the 2 types of neuron as a function of test voltage, shown on natural log scale. Values were significantly different at 10, 30, and 40 mV ($P < 0.05$). Values at 0 and 20 mV were not significantly different ($P > 0.05$). Average values for linear regression fits to individual data sets are, for sympathetic neurons: slope = -0.039 ± 0.003, intercept = 0.79 ± 0.06, $n = 6$; for pyramidal neurons: slope = -0.047 ± 0.004, intercept = 0.65 ± 0.08, $n = 7$. Slopes and intercepts are not significantly different ($P > 0.05$). *D*: deactivation speeds of native and cloned N-type channels. The three pairs of bars indicate average deactivation time constants of native N-type channels (native) and 2 $Ca_V2.2$ splice isoforms co-expressed with $Ca_V\beta_3$ and $Ca_V\alpha_2\delta$ ($\alpha_{2\delta}/\beta_3$), and with $Ca_V\beta_3$ only (β_3). Data from hippocampal pyramidal neurons is represented by ■ ($n = 8$) and sympathetic neurons by ▨ ($n = 6$). For clones expressed with and without $Ca_V\alpha_2\delta$, data from the $Ca_V2.2$e[24a, Δ31a] isoform is represented by ■ and $Ca_V2.2$e[Δ24a, 31a] by ▨. *, that values are significantly different ($P < 0.05$). Data are means ± SE. Deactivation speeds, all recorded at −60 mV (including correction for surface charge screening).

activation of voltage-gated channels, including calcium channels, invoke a final voltage-independent conformational closed-open step that is rate limiting at sufficiently strong depolarizations (Chen and Hess 1990; Frazier et al. 2001; Zagotta et al. 1988). We observed kinetic differences between S3 and S4 splice isoforms over a range of voltages while steady-state activation curves for both gating and ionic currents were not distinguishable between isoforms. These observations are consistent with the involvement of a gating transition closely linked to the open state perhaps in the final voltage-independent closed-open transition.

Summary

The mammalian $Ca_v2.2$ gene is encoded by ≥50 exons, ≥10 of which can be alternatively spliced. In addition to exons 24a and 31a, alternative splicing involves exon 10 in the I–II intracellular loop, exons 18a, 19, 20, and 21 in the II–III intracellular loop, and exons 37a/37b, and 46 in the C terminus (Lipscombe and Castiglioni 2004). It is therefore important to note that there is no one peripheral or central form of the $Ca_V2.2$ gene. Indeed, our recent single-cell RT-PCR analysis shows that even individual neurons of the dorsal root ganglia express multiple $Ca_V2.2$ splice isoforms (Bell et al. 2004). Significantly, however, of the 10 sites of alternative splicing that have been identified so far in mammalian $Ca_V2.2$ genes (Lipscombe and Castiglioni 2004), only exon 31a is restricted to peripheral neurons; based on our recent single-cell RT-PCR analysis in dorsal root ganglia, exon 31a is present in every $Ca_V2.2$ mRNA (Bell et al. 2004). Collectively, our studies are therefore consistent with the conclusion that tissue-specific expression of exon 31a of $Ca_V2.2$ underlies the comparatively slow kinetics of N-type calcium channels in peripheral neurons. Pharmacological tools to discriminate between these splice isoforms would help establish their relative contribution to synaptic events. The *Conus* peptides tested here did not differentiate between splice isoforms, although others have reported differential effects of *Conus catus*, peptides under

certain conditions (Lewis et al. 2000). The voltage dependence of the two splice forms in mammalian cells are equal, therefore pharmacological strategies to distinguish between them would probably need to exploit the different binding epitopes in the S3-S4 linkers directly. The cell lines developed here provide useful tools for studying splice isoforms of the N-type Ca channel that exhibit properties similar to those of native currents (Barrett et al. 2001) and with current densities sufficiently high to monitor gating currents.

ACKNOWLEDGMENTS

We thank A. J. Castiglioni for helpful comments on the manuscript.

Present address of S. I. McDonough: Amgen, Inc., 1 Amgen Center Dr., mailstop 29-2-B, Thousand Oaks, CA 91320-1799.

GRANTS

This work was supported by National Institutes of Health Grants NS-29967 to D. Lipscombe and P41RR-01395 to S. I. McDonough and a grant from the American Heart Association to S. I. McDonough.

REFERENCES

Barrett CF, Liu L, and Rittenhouse AR. Arachidonic acid reversibly enhances N-type calcium current at an extracellular site. *Am J Physiol Cell Physiol* 280: C1306–1318, 2001.

Barry EL, Gesek FA, Froehner SC, and Friedman PA. Multiple calcium channel transcripts in rat osteosarcoma cells: selective activation of alpha 1D isoform by parathyroid hormone. *Proc Natl Acad Sci USA* 92: 10914–10918, 1995.

Bell TJ, Thaler C, Castiglioni AJ, Helton TD, and Lipscombe D. Cell-specific alternative splicing increases calcium channel current density in the pain pathway. *Neuron* 41: 127–138, 2004.

Bezanilla F. The voltage sensor in voltage-dependent ion channels. *Physiol Rev* 80: 555–592, 2000.

Birnbaumer L, Qin N, Olcese R, Tareilus E, Platano D, Costantin J, and Stefani E. Structures and functions of calcium channel beta subunits. *J Bioenerg Biomembr* 30: 357–375, 1998.

Black DL. Protein diversity from alternative splicing: a challenge for bioinformatics and post-genome biology. *Cell* 103: 367–370, 2000.

Bourinet E, Soong TW, Sutton K, Slaymaker S, Mathews E, Monteil A, Zamponi GW, Nargeot J, and Snutch TP. Splicing of alpha 1A subunit gene generates phenotypic variants of P- and Q-type calcium channels. *Nat Neurosci* 2: 407–415, 1999.

Chen CF, and Hess P. Mechanism of gating of T-type calcium channels. *J Gen Physiol* 96: 603–630, 1990.

Colquhoun D. Practical analysis of single channel records. In: *Microelectrode Techniques* (2nd ed.), edited by Ogden D. Cambridge, UK: The Company of Biologists, 1994, p. 101–139.

Ertel EA, Campbell KP, Harpold MM, Hofmann F, Mori Y, Perez-Reyes E, Schwartz A, Snutch TP, Tanabe T, Birnbaumer L, Tsien RW, and Catterall WA. Nomenclature of voltage-gated calcium channels. *Neuron* 25: 533–535, 2000.

Frazier CJ, Serrano JR, George EG, Yu X, Viswanathan A, Perez-Reyes E, and Jones SW. Gating kinetics of the alpha1I T-type calcium channel. *J Gen Physiol* 118: 457–470, 2001.

Garcia J, Gerber SH, Sugita S, Sudhof TC, and Rizo J. A conformational switch in the Piccolo C2A domain regulated by alternative splicing. *Nat Struct Mol Biol* 11: 45–53, 2004.

Grabowski PJ. Splicing regulation in neurons: tinkering with cell-specific control. *Cell* 92: 709–712, 1998.

Hans M, Urrutia A, Deal C, Brust PF, Stauderman K, Ellis SB, Harpold MM, Johnson EC, and Williams ME. Structural elements in domain IV that influence biophysical and pharmacological properties of human alpha1A-containing high-voltage-activated calcium channels. *Biophys J* 76: 1384–1400, 1999.

Helton TD, Kojetin DJ, Cavanagh J, and Horne WA. Alternative splicing of a Beta 4 subunit proline-rich motif regulates voltage-dependent gating and toxin block of cav2.1 Ca^{2+} channels. *J Neurosci* 22: 9331–9339, 2002.

Hering S. beta-Subunits: fine tuning of Ca(2+) channel block. *Trends Pharmacol Sci* 23: 509–513, 2002.

Hille B, Woodhull AM, and Shapiro BI. Negative surface charge near sodium channels of nerve: divalent ions, monovalent ions, and pH. *Philos Trans R Soc Lond B Biol Sci* 270: 301–318, 1975.

Ihara Y, Yamada Y, Fujii Y, Gonoi T, Yano H, Yasuda K, Inagaki N, Seino Y, and Seino S. Molecular diversity and functional characterization of voltage-dependent calcium channels (CACN4) expressed in pancreatic beta-cells. *Mol Endocrinol* 9: 121–130, 1995.

Ikeda SR and Dunlap K. Voltage-dependent modulation of N-type calcium channels: role of G protein subunits. *Adv Second Messenger Phosphoprotein Res* 33: 131–151, 1999.

Jiang Y, Lee A, Chen J, Ruta V, Cadene M, Chait BT, and MacKinnon R. X-ray structure of a voltage-dependent K^+ channel. *Nature* 423: 33–41, 2003.

Jones LP, DeMaria CD, and Yue DT. N-type calcium channel inactivation probed by gating-current analysis. *Biophys J* 76: 2530–2552, 1999.

Jones LP, Patil PG, Snutch TP, and Yue DT. G-protein modulation of N-type calcium channel gating current in human embryonic kidney cells (HEK 293). *J Physiol* 498: 601–610, 1997.

Jones LP, Wei SK, and Yue DT. Mechanism of auxiliary subunit modulation of neuronal alpha1E calcium channels. *J Gen Physiol* 112: 125–143, 1998.

Krovetz HS, Helton TD, Crews AL, and Horne WA. C-Terminal alternative splicing changes the gating properties of a human spinal cord calcium channel alpha 1A subunit. *J Neurosci* 20: 7564–7570, 2000.

Lewis RJ, Nielsen KJ, Craik DJ, Loughnan ML, Adams DA, Sharpe IA, Luchian T, Adams DJ, Bond T, Thomas L, Jones A, Matheson JL, Drinkwater R, Andrews PR, and Alewood PF. Novel omega-conotoxins from *Conus catus* discriminate among neuronal calcium channel subtypes. *J Biol Chem* 275: 35335–35344, 2000.

Ligon B, Boyd AE 3rd, and Dunlap K. Class A calcium channel variants in pancreatic islets and their role in insulin secretion. *J Biol Chem* 273: 13905–13911, 1998.

Lin Z, Haus S, Edgerton J, and Lipscombe D. Identification of functionally distinct isoforms of the N-type Ca^{2+} channel in rat sympathetic ganglia and brain. *Neuron* 18: 153–166, 1997.

Lin Z, Lin Y, Schorge S, Pan JQ, Beierlein M, and Lipscombe D. Alternative splicing of a short cassette exon in alpha1B generates functionally distinct N-type calcium channels in central and peripheral neurons. *J Neurosci* 19: 5322–5331, 1999.

Lipscombe D and Castiglioni, A. J. Alternative splicing in voltage-gated calcium channels. Calcium Channel Pharmacology. In: *Calcium Channel Pharmacology* (1st ed.), edited by McDonough SI. New York: Kluwer/Academic/Plenum, 2004, p. 369–409.

Lipscombe D, Pan JQ, and Gray AC. Functional diversity in neuronal voltage-gated calcium channels by alternative splicing of Ca(v)alpha1. *Mol Neurobiol* 26: 21–44, 2002.

McDonough SI. Peptide toxin inhibition of voltage-gated calcium channels: selectivity and mechanisms. In: *Calcium Channel Pharmacology* (1st ed.), edited by McDonough SI. New York: Kluwer/Academic/Plenum Publishing, 2004, p. 95–142.

McDonough SI, Mintz IM, and Bean BP. Alteration of P-type calcium channel gating by the spider toxin omega-Aga-IVA. *Biophys J* 72: 2117–2128, 1997.

Nakai J, Adams BA, Imoto K, and Beam KG. Critical roles of the S3 segment and S3-S4 linker of repeat I in activation of L-type calcium channels. *Proc Natl Acad Sci USA* 91: 1014–1018, 1994.

Noceti F, Baldelli P, Wei X, Qin N, Toro L, Birnbaumer L, and Stefani E. Effective gating charges per channel in voltage-dependent K^+ and Ca^{2+} channels. *J Gen Physiol* 108: 143–155, 1996.

Pan JQ and Lipscombe D. Alternative splicing in the cytoplasmic II-III loop of the N-type Ca channel alpha 1B subunit: functional differences are beta subunit-specific. *J Neurosci* 20: 4769–4775, 2000.

Peixoto AA, Smith LA, and Hall JC. Genomic organization and evolution of alternative exons in a *Drosophila* calcium channel gene. *Genetics* 145: 1003–1013, 1997.

Perez-Reyes E, Wei XY, Castellano A, and Birnbaumer L. Molecular diversity of L-type calcium channels. Evidence for alternative splicing of the transcripts of three non-allelic genes. *J Biol Chem* 265: 20430–20436, 1990.

Scott VE, De Waard M, Liu H, Gurnett CA, Venzke DP, Lennon VA, and Campbell KP. Beta subunit heterogeneity in N-type Ca^{2+} channels. *J Biol Chem* 271: 3207–3212, 1996.

Smith LA, Peixoto AA, Kramer EM, Villella A, and Hall JC. Courtship and visual defects of cacophony mutants reveal functional complexity of a calcium-channel alpha1 subunit in *Drosophila*. *Genetics* 149: 1407–1426, 1998.

Smith LA, Wang X, Peixoto AA, Neumann EK, Hall LM, and Hall JC. A *Drosophila* calcium channel alpha1 subunit gene maps to a genetic locus associated with behavioral and visual defects. *J Neurosci* 16: 7868–7879, 1996.

Snutch TP, Tomlinson WJ, Leonard JP, and Gilbert MM. Distinct calcium channels are generated by alternative splicing and are differentially expressed in the mammalian CNS. *Neuron* 7: 45–57, 1991.

Starr TV, Prystay W, and Snutch TP. Primary structure of a calcium channel that is highly expressed in the rat cerebellum. *Proc Natl Acad Sci USA* 88: 5621–5625, 1991.

Stotz SC and Zamponi GW. Identification of inactivation determinants in the domain IIS6 region of high voltage-activated calcium channels. *J Biol Chem* 276: 33001–33010, 2001.

Takimoto K, Li D, Nerbonne JM, and Levitan ES. Distribution, splicing and glucocorticoid-induced expression of cardiac alpha 1C and alpha 1D voltage-gated Ca^{2+} channel mRNAs. *J Mol Cell Cardiol* 29: 3035–3042, 1997.

Wakamori M, Mikala G, and Mori Y. Auxiliary subunits operate as a molecular switch in determining gating behaviour of the unitary N-type Ca^{2+} channel current in *Xenopus* oocytes. *J Physiol* 517: 659–672, 1999.

Walker D and De Waard M. Subunit interaction sites in voltage-dependent Ca^{2+} channels: role in channel function. *Trends Neurosci* 21: 148–154, 1998.

Witcher DR, De Waard M, Sakamoto J, Franzini-Armstrong C, Pragnell M, Kahl SD, and Campbell KP. Subunit identification and reconstitution of the N-type Ca^{2+} channel complex purified from brain. *Science* 261: 486–489, 1993.

Zagotta WN, Brainard MS, and Aldrich RW. Single-channel analysis of four distinct classes of potassium channels in *Drosophila* muscle. *J Neurosci* 8: 4765–4779, 1988.